ELSEVIER

Astroparticle Physics 7 (1997) 343–356

Astroparticle Physics

Correlated features of arrival time and angle-of-incidence distributions of EAS muons

I.M. Brâncus [1], B. Vulpescu [1], H. Rebel *, M. Duma [1], A.A. Chilingarian [2]

Forschungszentrum Karlsruhe, Institut für Kernphysik, P.O.B. 3640, D 76021 Karlsruhe, Germany

Received 21 April 1997; accepted 14 June 1997

Abstract

Various features and correlations of the arrival time and angle-of- incidence distributions of muons of extensive air showers (EAS) are studied by analyses based on Monte-Carlo simulations of the EAS development by using the air shower simulation code CORSIKA. Trends and dependencies of the temporal dispersion of the EAS muon component on shower size and distance from the shower core are displayed by the distribution of the arrival time and angle of incidence of the first muon, of the mean and median of the single shower distribution. Special attention is called to multi-correlations in observations at different radial distances from the shower core. These 'radial' correlations provide additional information for the discrimination of different EAS primaries, while the correlation of muon arrival time and angle-of-incidence is shown to improve the mass separation only insignificantly. This feature does not basically change, when arrival times and angles of incidence are displayed by transformed quantities like 'muon production heights'. © 1997 Elsevier Science B.V.

1. Introduction

The contemporary interest in a detailed understanding of the longitudinal development of extensive air showers (EAS), induced by high-energy primary cosmic rays, arises from the possibilities of learning about the nature of the cosmic particle interacting with the air nuclei and about the interaction mechanisms at ultrahigh energies. Since the pioneering work in the 1950s [1], the temporal and spatial structure of the EAS disc, observed at a certain observation level, i.e. the lateral, the arrival time and angle-of-incidence distributions of the different EAS components are considered to be a source of information relevant for these aspects.

In particular, due to the high penetrability of muons and Cerenkov photons, the temporal dispersion of the muon component [2] and the shape of the Cerenkov pulse [3] are considered to map rather directly the history and geometrical structure of the shower development [4].

Though EAS muons are much less abundant than the Cerenkov photons, their observation provides some advantages since the muons are more directly coupled to the interactions of the leading particle and as they can be observed 24 hours per day. The features of the muon case have been explored by systematic experimental studies [5–13], in particular with the water-Cerenkov detector installation of the Haverah Park.

More recently various aspects of muon arrival time and angle-of-incidence distributions have been

* Corresponding author. E-mail: rebel@ik3.fzk.de.

[1] Permanent address: IFIN-HH, P.O.B. MG 6, RO – 7690 Bucharest, Romania.

[2] Permanent address: Yerevan Physics Institute, Cosmic Ray Dept., Alikhanyan Brothers Str. 2, Yerevan 36, Armenia.

0927-6505/97/$17.00 © 1997 Elsevier Science B.V. All rights reserved.
PII S0927-6505(97)00030-3

detailed in view of particular specific EAS observation projects and (proposed) experimental devices [14–21]. In the context of detection facilities of the KASCADE central detector, Rebel et al. [17] directed the interest to the shape and position of various kinds of muon arrival distributions, their dependence on the shower size N_e, the radial distance R_μ from the shower center and on the mass of the primaries, looking for discriminating features as signatures of the mass of the cosmic ray primaries. The studies include the detector performance and introduce advanced statistical methods for analyzing the 'observed' multivariate distributions (see also [21]). Danilova et al. [18] analyzed the spatial angle-of-incidence and the arrival time distributions of EAS muons in order to relate them to the longitudinal profile of the muon cascade and to determine the production heights. Following ideas of McComb and Turver [22] and of Linsley [23], the 'Time-Track-Complementary' approach (see also [19]) has been worked out, based on the correlation of the temporal and spatial characteristics of the muon component.

The present paper reports EAS simulation analyses, focused to a further exploration of the role of correlation features which may be observed together with muon arrival time and angle-of-incidence distributions. To prepare a coherent basis of the analyses, we consider hypothetical muon timing-tracking detectors of $10 * 10$ m^2 area with ideal detection qualities. Special attention is paid to multicorrelations of shower variables, which are observed by a set of such detectors located at several different distances from the shower center. The studies reveal interesting features of correlated distributions, which are corroborated by nonparametric multivariate analyses techniques [24,25].

2. EAS simulation data

The set of data of simulated EAS, induced by p, O and Fe primaries, is identical with that used in [17], enlarged by oxygen-initiated EAS and calculated for nine values of the primary energy E_0 in equidistant steps of the log E_0 scale between 10^{14} and 10^{16} eV and grouped in nine groups of the shower size, taking into account the realistic slope of the primary energy spectrum. It should be recalled that a definite shower size bin corresponds to different bins of the primary energy for different mass primaries, with generally smaller shower sizes and smaller fluctuations for the heavier particle of a definite energy (see [21] e.g.). All simulations have been performed with the air-shower Monte-Carlo simulation program CORSIKA [26], which has been specifically developed in the context of the KASCADE experiment and is under continuous refinement of the hadronic interaction models used as Monte-Carlo generators at ultrahigh energies. A comparison of various features of the currently used models is given by a recent account and updating of the CORSIKA code [27]. All secondary particles are tracked explicitly along their trajectories, and their parameters are stored on tape when reaching the observation level (in the present case 110 m a.s.l.). This allows a detailed analysis of all features of the simulated data. For sake of simplicity the present exploration studies consider showers of vertical incidence only. Some characteristic features of various types EAS muon distributions of typical proton and Fe induced showers of $E = 10^{15}$ eV are illustrated by displays in [28].

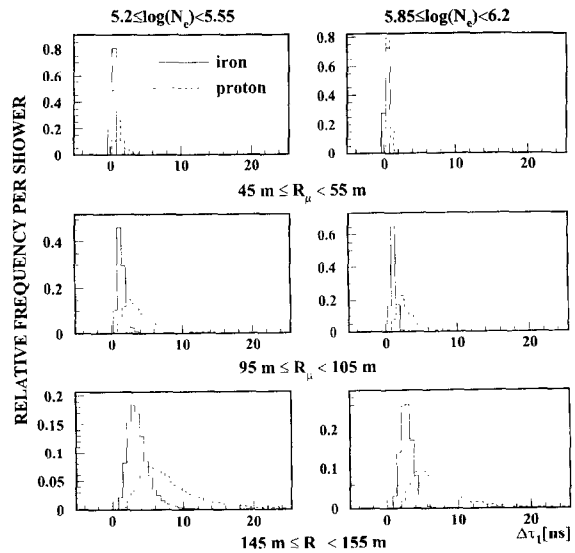

Fig. 1. Distributions of the relative arrival times of the foremost muons originating from proton and iron induced EAS, observed for different shower sizes and radial distances from the shower center.

3. Arrival time and angle of incidence distributions of EAS muons

The origin of the sensitivity of muon arrival times to the mass of the interaction and nature of the primary results from differences of the longitudinal EAS development due to differences in the interaction length, in the transverse momentum distributions of the secondaries and inelasticities. In a simple approximation, through the time-of-flight of the muons, the arrival times map the production in high altitudes. In an analogous way the angles-of-incidence reflect the direction of the muon travel, pointing to the production loci on (or near) the shower axis.

Thus the structures of muon arrival time distributions depend on the mass and the energy of the primary (shower size N_e, respectively), from EAS arrival direction, on the radial distance R_μ from the shower center of the muon observation, on the energy threshold and multiplicity of the muon observation. Under these aspects they have been already considered in various investigations [14–19,21]. Recently, in view of the KASCADE facilities [15], simulated proton and Fe induced EAS of vertical incidence have been extensively analyzed to prepare for corresponding measurements [17]. In addition to the distribution of the mean values of the muon arrival times of the single showers

$$\Delta\tau_{mean} = \tau_\mu(R_\mu) - \tau_c \tag{3.1}$$

(τ_c = arrival time of the shower in the center), the distributions of the arrival times

$$\Delta\tau_1 = \tau_\mu^1(R_\mu) - \tau_c \tag{3.2}$$

of the earliest or foremost muon (with high probability of originating from an early stage of the shower

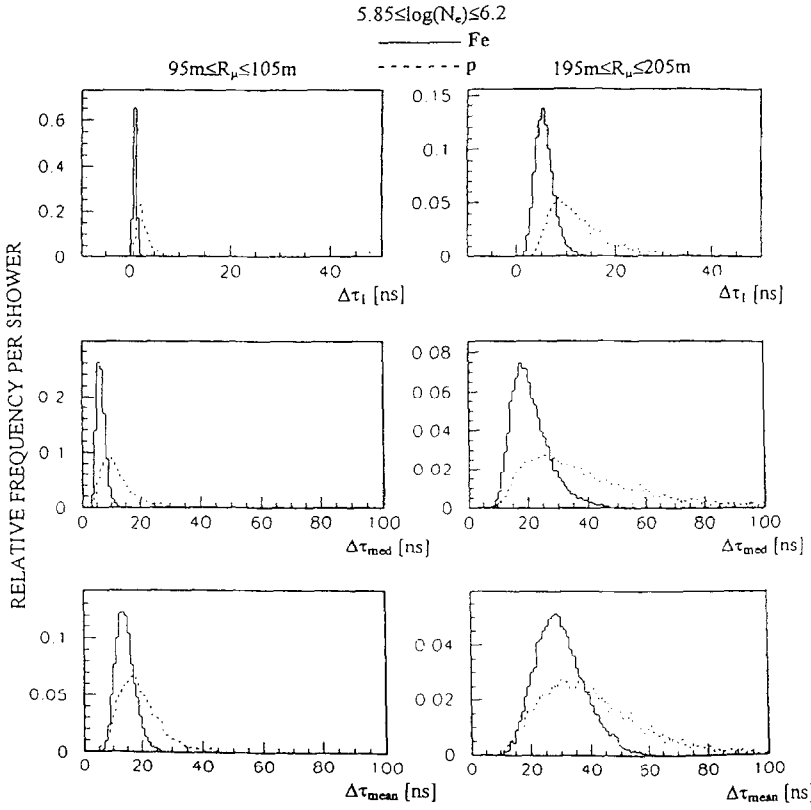

Fig. 2. Comparison of the distributions of the arrival times of the foremost muons with the distributions of the mean and median values of the single EAS distributions, displayed for two different radial distances of the muon observation.

development), triggered by 4 subsequently registered muons with $E_\mu \geq 2$ GeV are studied. The present paper follows these studies and adds the studies of oxygen induced showers, using a different threshold energy of 1.0 GeV and occasionally also considering the median values

$$\Delta\tau_{\text{med}} = \tau_\mu^{\text{med}}(R_\mu) - \tau_c \qquad (3.3)$$

of the distributions [21]. The median value appears to be of specific use to suppress the influence of large fluctuations from typical values and is expected to be especially useful in experiments when one timing detector shows malfunctional offset.

The analyses reproduce the general features of arrival time and angle-of-incidence distributions of EAS muons, studied for different primaries of different shower sizes and observed at different distances of the detector setups from the shower center (Fig. 1). The results are for a hypothetical array of detectors of $10 * 10$ m^2 area each, positioned within 10 m broad radial bins in various distances from the shower center, and for an energy threshold $E_\mu \geq 1$ GeV for the detected muons. The average shifts and the broadening of the distributions with increasing distance from the shower center [29] show trends similar to those observed with all charged particles [14]. Comparing different types of primaries the distributions are distinctly shifted, with smaller widths, to smaller arrival times and angles-of-incidence of the muons for the heavier primaries, which reflects the shorter interaction lengths and smaller fluctuations of the heavier projectile.

Fig. 2 compares the distributions of $\Delta\tau_1$, of $\Delta\tau_{\text{mean}}$ and $\Delta\tau_{\text{med}}$, indicating some advantages of the obser-

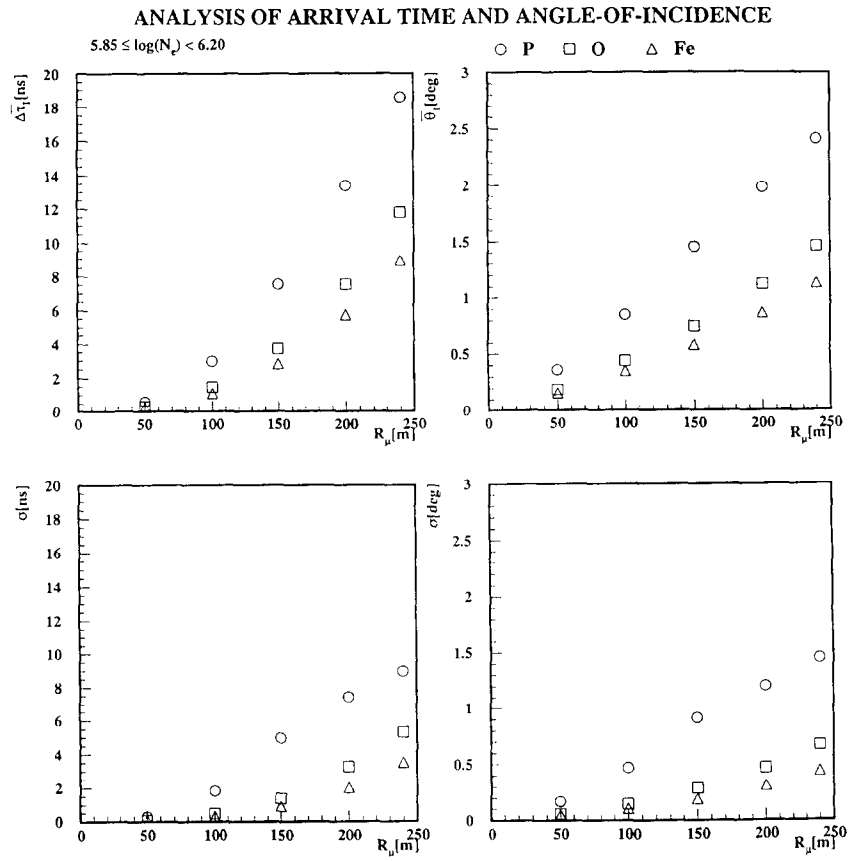

Fig. 3. Mean and standard deviation of the arrival time distributions of the foremost muons: Dependence on the distance from the shower center ($5.85 \leq \log N_e \leq 6.20$).

vation of the first muons. This is due to the fact that in this way higher energy muons, generated in the first interactions, are preferentially selected [17].

Fig. 3 compiles for two primaries the dependence of the average shifts (of the distributions of $\Delta\tau_1$), and of the corresponding widths σ, on the distance from the shower center. It should be noted that these dependencies vary with the energy threshold of muon detection [21,30].

4. Correlated distributions

In previous studies of muon arrival time distributions [17,18] single distributions, observed at several distances from EAS center, have been analyzed in view of the information of the mass of the primary cosmic particles. The muon multiplicity N_μ, more precisely the ratio N_μ/N_e is considered to be a powerful signature for the nature of the primary. In fact, the correlation with any number of muons (e.g. that observed with the available and always limited detector area) is expected to enhance the separation quality. This has been shown for the arrival time distributions in [17,29], also studying the role of correlations with the shower age. The correlation

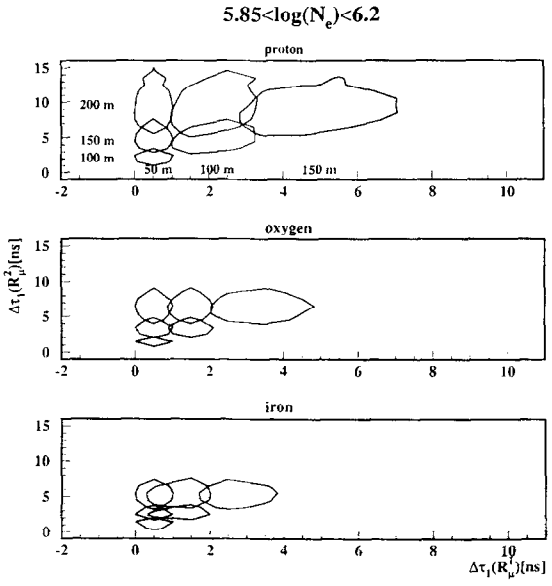

Fig. 4. Correlation of the arrival times of the foremost muons observed at different radial distances for proton, oxygen and iron induced EAS: the contours displays the half maximum of the distributions.

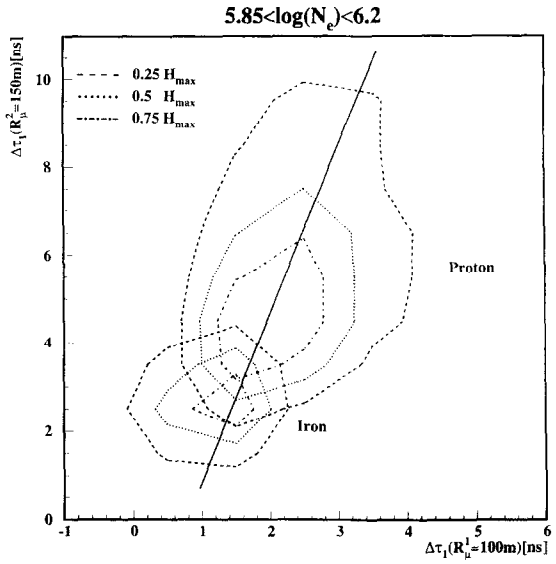

Fig. 5. Correlation of the arrival times of the foremost muons of proton and iron induced EAS, observed with two detectors placed at 100 m and 150 m distance from the shower center. The straight line connects the maxima, and the distributions projected on this axis, can be disentangled anticipating the shape of the different contributions [21].

with a specific part of the total muon intensity has been also adopted as additional discriminant in some other recent work [19], starting from simultaneous considerations of arrival times and angles-of-incidence [18]. The complementary features of arrival time distributions with the angle-of-incidence distributions have been worked out in detail as a source of information on the longitudinal development of the air showers [18]. However, the role of the so called Time-Track-Complementary (TTC) principle in analyzing the mass composition of cosmic rays has not been sufficiently critically analyzed. Using nonparametric statistical analyses techniques we will briefly address this item (Section 5).

In this section we display some correlations of different shower parameters with the muon arrival time distributions and extend previous studies with a special focus of correlating observations at different distances from the shower core. Figs. 4 and 5 reveal the correlations of the arrival times for muons (shown for the foremost muons) from proton, oxygen and iron induced showers observed at different distances from the shower core. The plots emphasize the strong dependence of the correlation from the R_μ^1–R_μ^2-com-

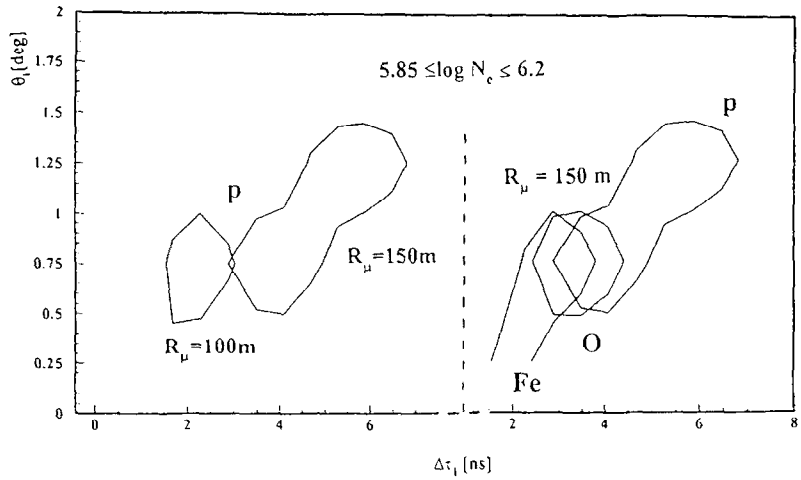

Fig. 6. Arrival times correlated with the angles-of-incidence of the first EAS muons of proton induced showers at two different distances, and for different primaries observed at the same distance from the shower center (shown are the contours of the half-maximum distributions).

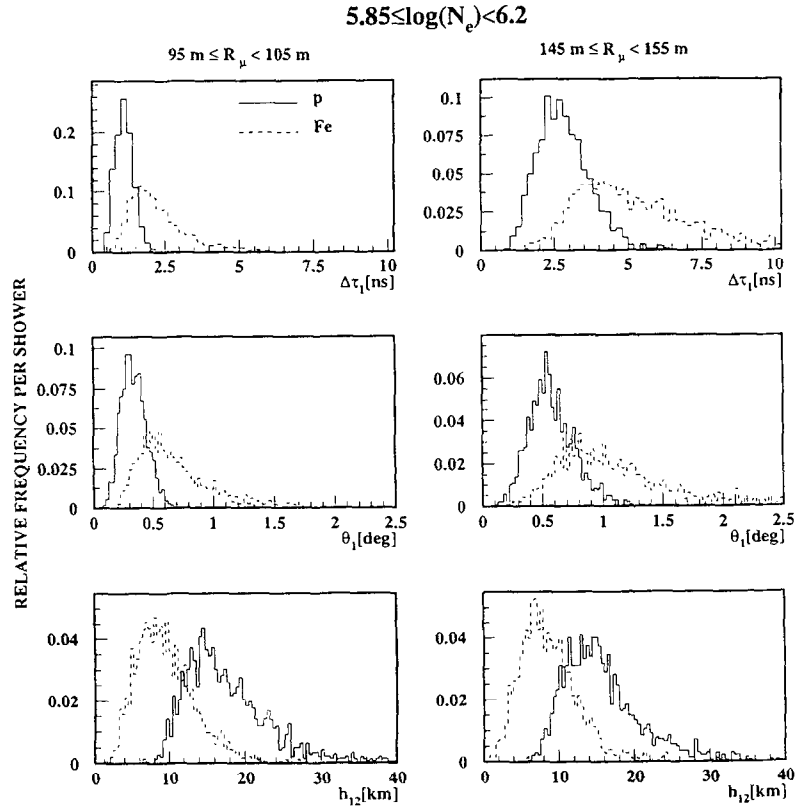

Fig. 7. Single distributions of the arrival time, angle-of-incidence and of the quantity h_{12} at R_μ = 100 m and at R_μ = 150 m for the foremost muons and for proton and iron induced showers.

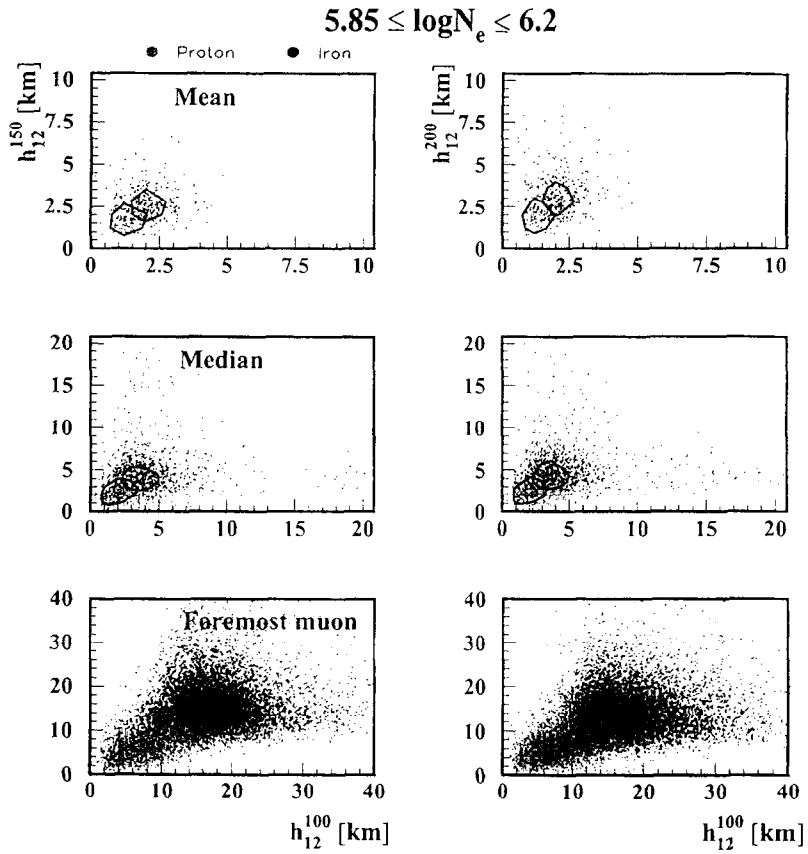

Fig. 8. Correlated distributions of h_{12} derived from two coincident timing-tracking observations at different instances R_μ for proton and iron induced showers, for the distributions of the foremost muons, of the median and mean values of the single distributions (shown are the contours of the half-maximum distributions.

bination and the pronounced dependence on the mass of the primary cosmic particle inducing EAS. There are analogous correlation features with similar information content for the distributions the angles-of-incidence Θ (measured relative to the shower axis) [21].

Fig. 6 illustrates the time-angle correlations dependent on different locations (R_μ) of the anticipated timing-tracking detector and on different primaries. The strong correlation of arrival time and angle-of-incidence distribution, finally formulated in the TTC principle is well known and the values of the correlation coefficient in the order of 0.9 [21] indicate that – apart from experimental aspects – observations of one quantity can be replaced by observations of the complementary one. This feature may be illustrated by a transformation of the arrival times and the angles-of-incidence to the so-called production heights of the muons. We introduce

$$\Delta\tau \to h_1 = \left(R_\mu^2 - (c\cdot\Delta\tau)^2\right)\Big/ 2c\Delta\tau, \quad \sigma_\tau \to \sigma_1, \tag{4.1}$$

$$\Theta \to h_2 = R_\mu/\tan\Theta, \quad \sigma_\Theta \to \sigma_2, \tag{4.2}$$

and define a correlation quantity

$$h_{12}(R_\mu) = \frac{h_1\sigma_1^2 + h_2\sigma_2^2 + r_{12}(h_1+h_2)\sigma_1\sigma_2}{\sigma_1^2 + \sigma_2^2 + 2r_{12}\sigma_1\sigma_2} \tag{4.3}$$

with correlation coefficient

$r_{12} = \sigma_{12}/\sigma_1\sigma_2$.

Actually, under simplified assumptions, neglecting multiple scattering and velocity dispersion effects e.g. these transformations relate $\Delta\tau_1$, or $\Delta\tau_{mean}$ and Θ_1, or Θ_{mean} to the geometrically reconstructed longitudinal development of the muon component, mapped by the h_1, h_2 or – condensed in one quantity – by h_{12} distributions.

Fig. 7 presents single distributions of the time, angle-of-incidence and quantity h_{12} at $R_\mu = 100$ m and at $R_\mu = 150$ m, for proton and iron induced showers corresponding to time and angle-of-incidence of the foremost muons.

Fig. 8 shows correlated distributions for two coincident time-tracking observations of h_{12} at different values of R_μ for proton and iron induced showers corresponding to time and angle-of-incidence of the foremost muons and for median and mean values, indicating an improved mass discrimination, when correlating different distances, in particular for the foremost-muon observation.

5. Application of nonparametric statistical analyses techniques

Multivariate analyses techniques facilitate the study of correlations between physical variables, the grouping of events by families and the comparison of experimental data with theoretical models. We use these techniques to explore the significance of the observed features for a discrimination of different EAS primaries, estimating the overlap of the multidimensional distributions and the misclassification by applying Bayesian decision rules [24,25]. Extending previous applications to the analysis of muon arrival time distributions [17] we scrutinize the above displayed features of arrival time and angle-of-incidence distributions, and in particular of their correlations.

5.1. The Bayesian approach

The analysis is focused to a statistical decision to associate a particular observed event v to a definite event class, say in our cases to proton or Fe-induced EAS. For that purpose we have to compare the a-posteriori probabilities P, i.e. the probabilities that if the observable takes a particular value v the primary is a proton or an iron nucleus.

$$P(\text{proton}/v) \lesseqgtr P(\text{Fe}/v)$$

$$\rightarrow \text{decision} \begin{cases} \text{Fe} \\ \text{proton} \end{cases} \tag{5.1}$$

The Bayesian decision rule consists in assigning the measured event v to the class given with the larger a-posteriori probability. This procedure introduces a quantification of the chance of a misclassification, associated with the smaller value of the a-posteriori probability.

From the multivariate histograms (of the considered observables), resulting from the Monte-Carlo simulations, we do infer conditional probability density distributions (*likelihood functions*)

$$P(v/p) \text{ and } P(v/\text{Fe})$$

of the observed events of a specified class. For an estimate of the a-posteriori probability the Bayes theorem is invoked, formulated with the notation of our example of discrimination Fe and proton primaries by

$$P(\text{Fe}/v) = \frac{p_{\text{Fe}}}{p_v} P(v/\text{Fe}), \tag{5.2}$$

$$P(\text{prot}/v) = \frac{p_{\text{prot}}}{p_v} P(v/\text{prot}). \tag{5.3}$$

Here p_{Fe}/p_v and p_{prot}/p_v are the initial assumptions about the probabilities (normalization: p_v) to observe an event of a specific class (a-priori *probabilities* by guesses which may be iterated in processing the analysis).

There are several procedures to prepare the likelihood functions from Monte-Carlo simulations (including neural network techniques). We use the most popular *Parzen window technique* [24] which substitutes each element of the training sample by bell-shaped functions and constructs the probability density by a superposition of many 'kernels'.

Fig. 9 displays examples of probabilities density distributions for the arrival time of the first EAS muon ($\Delta\tau_1$) derived from the training samples.

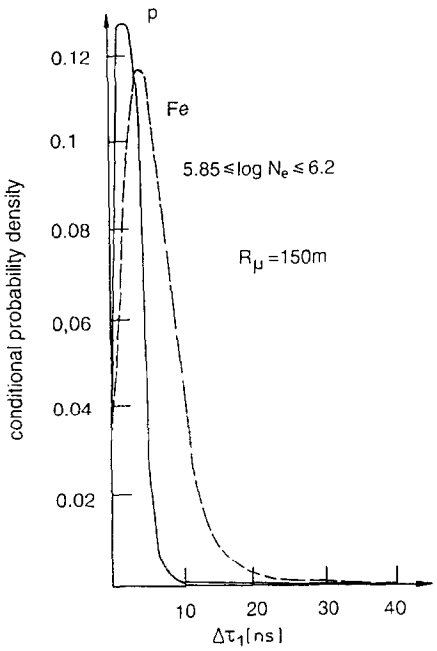

Fig. 9. Probability density distributions for the arrival time of the first muon for proton and Fe EAS primaries, shown for the case of $R_\mu = 150$ m and log $N_e = 5.85 - -6.2$.

The chance of misclassifying a particular observed event v_α due to the overlap of the likelihood functions is given by

$$r(v_\alpha) = \mathrm{Min}\{P(\mathrm{proton}/v_\alpha), P(\mathrm{Fe}/v_\alpha)\} \qquad (5.4)$$

and the Bayes error, indicating the chance of misclassifying the events of the observation space

$$R = \int_v r(v) P(v)\, dv. \qquad (5.5)$$

For an estimate of the Bayes error we use the method of the 'one-leave-out-for-a-time' test [23] which removes one element of the sample and trains the sample without it. The element is subsequently classified and returned into the sample. Thus, using the definition

$$\varepsilon(v) = \begin{cases} 0 & \text{if classified correctly,} \\ 1 & \text{otherwise,} \end{cases} \qquad (5.6)$$

the estimate is

$$R^e = \frac{1}{M} \sum_e^M \varepsilon(v_e) \qquad (5.7)$$

This estimate could be done for each class: m = proton, Fe, ... separately

$$R_m^e = \frac{1}{M_m} \sum_e^{M_m} \varepsilon(v_e^m). \qquad (5.8)$$

5.2. Classification results

The classification and misclassification of a particular event depends on the extent to which the probability distribution overlaps with the distributions of the alternative cases. In the following we present some illustrative results of the analysis of the arrival time ($\Delta\tau_1$) and angle-of-incidence (Θ_1) distributions of the foremost muons, observed at distances $R_\mu \geq 100$ m and in particular, for the highest log N_e bin: 5.85–6.20 considered. Three different EAS primaries are taken into account.

The main conclusions of the results of the classification procedure are (see also [21]):

- The observation of the time-angle correlation does not improve the mass discrimination inferred from the arrival time and angle-of-incidence distributions separately.
- Reconstructing the muon production heights and mapping the longitudinal development of EAS using procedures, proposed in [18], do not reveal additional information about the mass of the primary as compared with the direct analysis muon time arrival distributions.
- The chance of misclassification and the Bayes error decrease with the shower size and the distance R_μ, but they increase with the complexity of the mass composition.

Fig. 10 indicates the classification probabilities for proton, O and Fe primaries derived from the shower age – arrival time – arrival time correlations, observed at two different radial distances (50 m, R_μ) of the foremost muons for two different log N_e ranges. The mass separation generally increases with the shower size or the primary energy, respectively.

Table 1 and Fig. 11 compile for the log N_e = 5.85–6.2 the classification and misclassification probabilities for various observation modes and emphasize the importance of observations which correlate arrival time (and analogously angles-of-incidence) distributions of different radial distances, with additional classification by the shower age. The mass

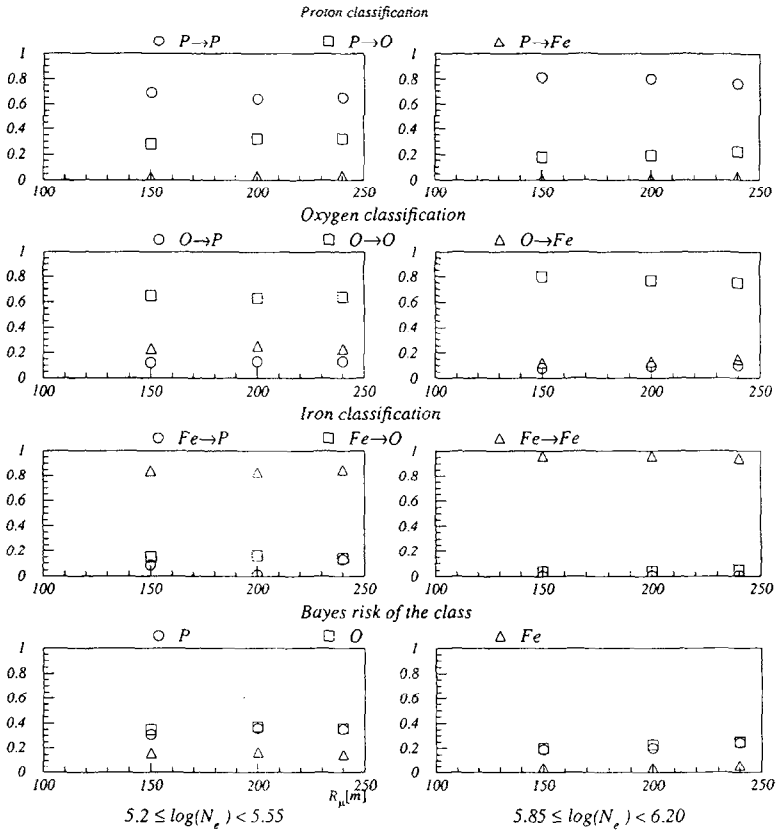

Fig. 10. True classification and misclassification probabilities with Bayes errors for proton, O and Fe primaries derived from observations of arrival time – arrival time-shower age correlations, observed at two different radial distances (50 m, R_μ) of the foremost muons, shown for two different log N_e ranges.

discrimination can be further improved, when additionally the multiplicity of the muons registrated with the detector [30] or even with the N_μ/N_e ratio [17] are correlated.

5.3. Reconstruction of the mass composition

Specified to the case of the three EAS primaries: p, O, Fe, we sketch a simple reconstruction procedure of the mass composition of a control sample with

$$N = n_p + n_O + n_{Fe}$$

events, using the classification ($P_{i \to i}$) and misclassification probabilities ($P_{j \to i}$) probabilities. The correct numbers of events of a specific class are altered by

$$\begin{aligned} n'_p &= P_{p \to p} n_p + P_{O \to p} n_O + P_{Fe \to p} n_{Fe}, \\ n'_O &= P_{p \to O} n_p + P_{O \to O} n_O + P_{Fe \to O} n_{Fe}, \\ n'_{Fe} &= P_{p \to Fe} n_p + P_{O \to Fe} n_O + P_{Fe \to Fe} n_{Fe}, \end{aligned} \tag{5.9}$$

which are interpreted as mean values of binomial distributions for the probability to find the particular class (i) among N realizations. Slightly generalizing the notation we write

$$n'_i = \sum_{j=1}^{3} n_j \cdot P_{ji}$$

Table 1
Classification probabilities using different sets of subvariables

Mode	p → p	p → O	p → Fe	O → p	O → O	O → Fe	Fe → p	Fe → O	Fe → Fe
$\Delta\tau_1$ (100 m)	0.73	0.23	0.04	0.13	0.40	0.47	0.004	0.15	0.85
h_{12} (100 m)	0.79	0.17	0.039	0.17	0.43	0.40	0.011	0.19	0.8
$\Delta\tau_1$ (100 m) − Θ_1 (100 m)	0.70	0.25	0.047	0.12	0.44	0.45	0.006	0.16	0.83
$\Delta\tau_1$ (100 m) − $\Delta\tau_1$ (150 m)	0.77	0.22	0.071	0.086	0.61	0.30	0.043	0.18	0.82
h_{12} (100 m) − h_{12} (150 m)	0.83	0.16	0.06	0.11	0.59	0.30	0.003	0.21	0.79
$\Delta\tau_1$ (100 m) − $\Delta\tau_1$ (150 m) − age	0.89	0.11	0.0	0.076	0.73	0.19	0.003	0.10	0.89

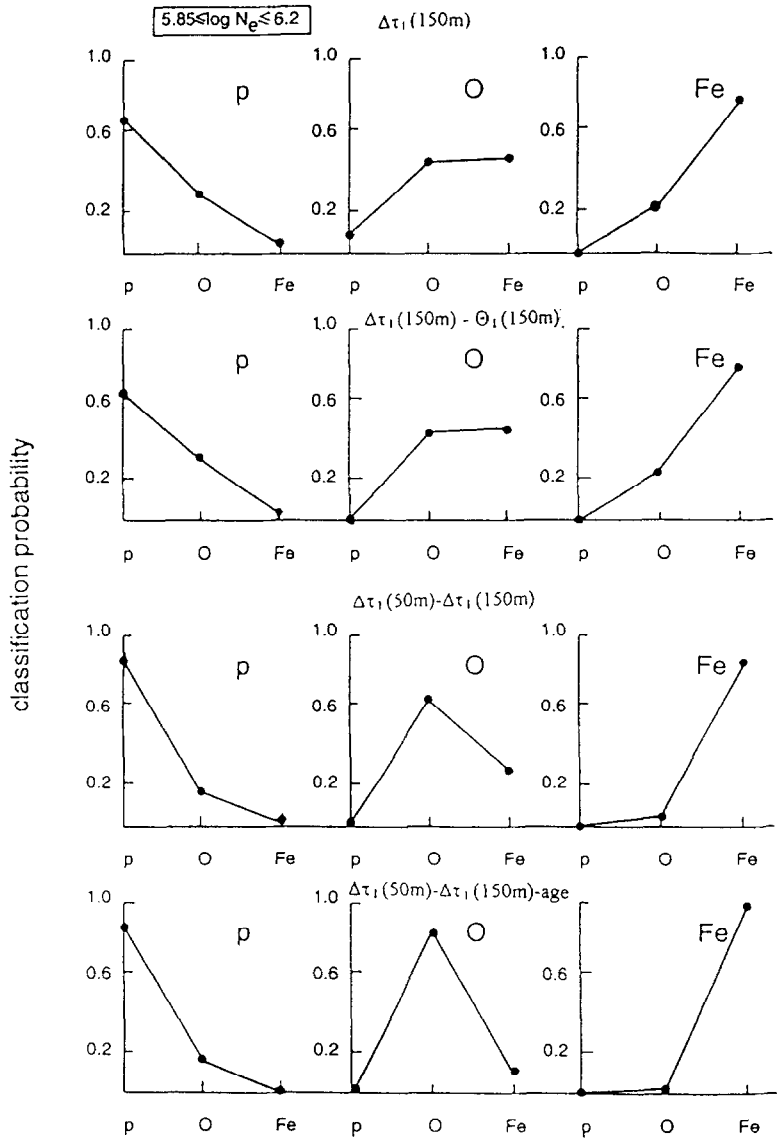

Fig. 11. Classification and misclassification probabilities for different observation modes.

Table 2
Results of the reconstruction procedure

Mode	p	O	Fe
$\Delta\tau_1$ (150 m)	4.68	3.31	3.23
$\Delta\tau_1$ (150 m) – Θ_1 (150 m)	4.49	3.33	3.12
$\Delta\tau_1$ (50 m) – $\Delta\tau_1$ (150 m)	5.74	2.37	2.88
$\Delta\tau_1$ (50 m) – $\Delta\tau_1$ (150 m) – age	5.75	2.18	3.07

with:

$$\sum_i^3 n_i' = \sum_j^3 n_j = N.$$

We consider the reconstruction of a 7:1:3 – p:O:Fe control sample of events induced by EAS in the N_e range: $5.85 \leq \log N_e \leq 6.20$ and express the results in terms of composition coefficients $C_i = n_i/N$.

Table 2 presents the reconstructed mass composition from results of various observation modes and displays again the role of the correlations. The errors in these values are dominated by the Bayes risk of the classification probabilities (as shown in Fig. 10, e.g.), while the uncertainty due to the binomial distribution of the n_i' values is practically negligible with sufficient large samples (N). This simple 'first guess' procedure can be improved by more complicated reconstruction methods [24], also elaborating realistic methodical errors.

6. Comments on TTC principle and on the mapping of production heights

The complementarity of arrival time and angle-of-incidence observations of EAS muons is in fact a strong correlation of both observables carrying nearly identical information content. Thus, apart from some practical aspects for consistency checks, both types of observations, when put together, do not provide independent information. As evidenced by Figure 15 a combined analysis does not improve the mass discrimination as compared to the analysis of one of these quantities separately, observed with equivalent accuracy. Naturally this feature is also not changed when the observables are transformed in 'muon production height' distributions, since the applied non-parametric inference technique already invokes the most favourable transformation in Mahalonobis space. It should be emphasized that due to the simplifications (e.g. Eqs. (4.1)–(4.3)) and a somehow arbitrary definition of the production height, the longitudinal development of the muon component is mapped with limited accuracy. Hence, when analyzing the mass composition, it appears hardly reasonable to introduce unnecessarily some additional uncertainties in a first step and subsequently to consider the transformed distributions for a further analysis.

Recently [19] the original concepts deriving information on mass of the primary from muon arrival time and angle-of-incidence distributions [17,18], in particular by simultaneous measurements of both types of observables have been modified. Thereby the term 'Time-Track-Complementary' is used in a sense different from that adopted in [18]. Referring to Eqs. (4.1)–(4.3), e.g., instead of analyzing the correlation quantity h_{12}, consistency of the two methods of production height determination, i.e. of the uncorrelated quantities h_1 and h_2 is required. Furthermore an additional discriminant is introduced: the fraction of muons generated above 500 g/cm^2 to the number of muons produced below 500 g/cm^2. However, whether this discriminant can be experimentally extracted with sufficient accuracy with a real detector of limited size, positioned at a certain distance from the shower center, is questionable. Moreover the bias and influence of the rather arbitrary muon selection criteria and of the $h_1 = h_2$ consistency condition (excluding most muons, perhaps predominantly those generated far-off the shower axis) on the selection of primary energies and mass are not understood and not demonstrated. Hence, with such a particular EAS selection of opaque bias, suppressing most of the experimental signal and displaying the longitudinal development of the muon component in a distorted way, the stated quality of the mass discrimination is misleading for real observations. Especially, the quoted misclassification rates of 10^{-4}–10^{-5} derived by a too simplified procedure (Gaussian approximation of the probability distributions) on the basis of poor statistics of only 200 events in total evidently appear most unrealistic.

7. Summary and conclusions

Studies of arrival time and angle-of-incidence distributions of muons from extensive air showers have

attracted considerable interest since they are considered to be a source of information on the longitudinal EAS development and on the mass composition of cosmic rays. This information potential has recently led to some interesting proposals [17–19] (in context with specific experimental installations), how dedicated experiments should be designed and analyzed, finally with the suggestion of setting up an array of 'muon-eyes' [16], potentially establishing observation capabilities analogous to the Fly' s Eye. The present studies pursue these aspects on the basis of realistic Monte-Carlo simulations (CORSIKA) of proton, oxygen and iron nuclei induced showers in the shower size range of log $N_e = 3.8–6.2$. First, the basic features of arrival time and angle-of-incidence distributions are recalled. Special attention is focused to simultaneous observations at different radial distances ('*radial correlations*'), which exhibit features improving the mass discrimination of the EAS primary. The identification of the primary mass has been attempted by a discriminant analysis, based on advanced nonparametric statistical analyses techniques and on a reconstruction procedure of the a-priori-assumed mass composition. In general, the main results can be characterised:

- Arrival time distributions and angle-of-incidence distributions show similar trends, improving the mass discrimination with increasing shower size N_e and observation distance from the shower core.
- As far as only the theoretical results of the simulations are considered (ignoring limitations by the detector qualities) the discrimination features are tentatively more pronounced by the distributions of the foremost arriving EAS muons rather than by the mean or median values of the distributions.
- There is a strong correlation of the muon arrival time distribution with the corresponding angle-of-incidence distribution, so that one type of measurements can be mutually fairly well replaced (or added for improving the statistical accuracy). This feature has been reported [18,19] as 'Time-Track-Complementarity'.
- However, due to the strong correlation, a combination of both type measurements does hardly improves the mass discrimination, and the application of timing or tracking or both combined is a matter of the experimental realization and mutual checks of systematic errors.
- In contrast 'radial correlations', i.e. correlated observations of the arrival time (angle-of-incidence) distributions at different distances from the shower center exhibit improvements in the mass discrimination, quantified by decreasing misclassification probabilities of the multivariate distribution analysis. A correlation with the shower age offers further distinct improvements, in addition to the observed muon multiplicity (see [30]).

Of course, the efficiency of radial correlations is increasing with the number of correlated variables and of setup detectors, located at different distances from the shower core. Thus, finally an experimental array measuring the temporal and directional characteristics of the arriving muon component along the lateral distribution in a radial sector of the shower disc would be of great interest.

Acknowledgements

The present results evolved from a continuous discussion of the merits of arrival time and angle-of-incidence measurements in context of the KASCADE approach. We acknowledge in particular, valuable discussions with Michelangelo Ambrosio, Florin Badea, Miriam Föller, Andreas Haungs, George Khristiansen, Hermann Josef Mathes, Jürgen Oehlschläger, Gerd Schatz, Samuel Ter-Antonyan, and Jürgen Wentz. We are grateful to Dieter Heck and Johannes Knapp for communicating us clarifying details of the CORSIKA simulations. Special thanks to Sabine Bucher for her patience in preparing the many iterations of the manuscript. Four of us (I.M.B., B.V., M.D. and A.A.C.) thank Forschungszentrum Karlsruhe for the hospitality during their research periods as visiting scientists, when most of the calculations have been done. The work has been partly supported by the International Bureau (Osteuropa – Verbindungsbureau) des BMBF Bonn on the basis of two WTZ projects of Forschungszentrum Karlruhe with IFIN-HH Bucharest, Romania and Yerevan Physics Institute, Armenia.

References

[1] P. Bassi, G. Clark, B. Rossi, Phys. Rev. 92 (1953) 441.
[2] J. Linsley, L. Scarsi, B. Rossi, Phys. Rev. Lett. 6 (1961) 485;

J. Linsley and L. Scarsi, Phys. Rev. 128 (1962) 2384; R. Thielert and L. Wiedecke, Z. Phys. 179 (1964) 199.
[3] Yu. Fomin, G.B. Khristiansen, Sov. J. Nucl. Phys. 14 (1971) 360; J.R. Patterson, A.M. Hillas, J. Phys. G: Nucl. Phys. 9 (1983) 327.
[4] I.M. Brâncus and H. Rebel, Proc. Tours Symposium on Nuclear Physics II, Tours, 30.8.–2.9.1994, France, p.78, eds. H. Utsunomiya, M. Ohta, J. Galin and G. Münzenberg.
[5] A.J. Baxter, A.A. Watson, J.G. Wilson, Canad. J. Phys. 46 (1968) S9.
[6] M.L. Armitage, P.R. Blake, W.F. Nash, J. Phys. A: Math. Gen. 8 (1975) 1005.
[7] R. Walker, A.A. Watson, J. Phys. G: Nucl. Phys. 7 (1981) 1297.
[8] P.R. Blake, W.S. Collis, M. Luksys, W.F. Nash, A.J. Septhon, J. Phys. G: Nucl. Phys. 16 (1990) 775.
[9] C.P. Woidneck, E. Böhm, J. Phys. A: Math. Gen. 8 (1975) 997.
[10] R.F. Kakimoto et al., J. Phys. G: Nucl. Phys. 9 (1983) 939; 12 (1986) 151.
[11] J. Linsley, J. Phys. G: Nucl. Phys. 12 (1986) 51.
[12] E.J. de Willier, D.J. van der Walt, P.K.F. Grieder, G. van Urk, J. Phys. G: Nucl. Phys. 12 (1986) 547.
[13] G.B. Khristiansen et al., 21th ICRC Adelaide (Australia), 9 (1990) 150.
[14] G. Agnetta et al., Nucl. Instr. Meth. A 359 (1995) 596; M. Ambrosio, C. Aramo, L. Colesanti, T.V. Danilova, A.D. Erlykin, Nucl. Phys. B (Proc. Suppl) 52B (1997) 225 – Proc. 9th ISVHECRI, Karlsruhe (Germany), 19–23 August 1996, eds. H. Rebel, G. Schatz, J. Knapp.
[15] P. Doll et al., Report KfK 4686 (1990), Kernforschungszentrum Karlsruhe – Nucl. Phys. B (Proc. Suppl.) A14 (1990) 336; H. Rebel – KASCADE collaboration, Proc. 7th ISVHECRI, Ann Arbor, Michigan, June 1992, AIP Conf. Proc. 276, p. 575, ed. L. Jones; G. Schatz – KASCADE collaboration, Proc. European Cosmic Ray Conference, Perpignan 1996, Nucl. Phys. B 53 (Proc. Suppl.) (1997) in press.
[16] D. Dumora, A.D. Erlykin, J. Procureur, J. Phys. G: Nucl. Part. Phys. 22 (1996) 273.
[17] H. Rebel, G. Völker, M. Föller, A.A. Chilingarian, J. Phys. G: Nucl. Part. Phys. 21 (1995) 451; H. Rebel, Proc. XV Cracow Summer School, Lodz (Poland), 15–19 July 1996, ed. W. Tkaczyk, in press.
[18] T.V. Danilova, D. Dumora, A.D. Erlykin, J. Procureur, J. Phys. G: Nucl. Part. Phys. 20 (1994) 961; Physics of Atomic Nuclei (Yadema Fizika) 59 (1996) 109.
[19] M. Ambrosio, C. Aramo, L. Colesanti, A.D. Erlykin, S.K. Machavariani, J. Phys. G: Nucl. Part. Phys. 23 (1997) 219; M. Ambrosio, C. Aramo, L. Colesanti, A.D. Erlykin, S.K. Machavariani, Nucl. Phys. B (Proc. Suppl.) 52B (1997) 225 – Proc. 9th ISVHECRI, Karlsruhe (Germany), 19–23 August 1996, eds. H. Rebel, G. Schatz, J. Knapp; M. Ambrosio, C. Aramo, L. Colesanti, A.D. Erlykin, S.K. Machavariani, Nucl. Phys. B (Proc. Suppl.) 52B (1997) 228 – Proc. 9th ISVHECRI, Karlsruhe (Germany), 19–23 August 1996, eds. H. Rebel, G. Schatz and J. Knapp.
[20] K. Berlöhr, Astropart. Phys. 5 (1996) 139.
[21] I.M. Brâncus, B. Vulpescu, H. Rebel, G. Völker, M. Duma, A.A. Chilingarian, Report FZK 5835 (1996), Forschungszentrum Karlsruhe.
[22] T.J.L. McComb, K.E. Turver, J. Phys. Soc. Japan 51 (1982) 3087.
[23] J. Linsley, 22nd ICRC, Dublin (Ireland), Conf. Abstr. 2 (1991) 873 – Nuovo Cim. 15C (1992) 321.
[24] A.A. Chilingarian, Comp. Phys. Comm. 54 (1989) 381; A.A. Chilingarian, G.Z. Zazian, Nuovo Cim. 14 (1991) 355.
[25] P. Desesquelles, Ann. Phys. Fr. 20 (1995) 1.
[26] J.N. Capdevielle et al., Report KfK 4998 (1992) Kernforschungszentrum Karlsruhe; J. Knapp, D. Heck, CORSIKA User's Manual, Report KfK 5196B (1993).
[27] J. Knapp, D. Heck, and G. Schatz, Report FZKA 5828 (1996), Forschungszentrum Karlsruhe; Nucl. Phys. B (Proc. Suppl.) 52B (1997) 136 – Proc. 9th ISVHECRI, Karlsruhe (Germany), 19–23 August 1996, eds. H. Rebel, G. Schatz and J. Knapp; D. Heck, J. Knapp, G. Schatz, Nucl. Phys. B (Proc. Suppl.) 52B (1997) 139 – Proc. 9th ISVHECRI, Karlsruhe (Germany), August 1996, eds. H. Rebel, G. Schatz, J. Knapp.
[28] H.J. Simonis, H. Rebel, Internal Report, Forschungszentrum Karlsruhe, 1996 unpublished.
[29] U. Raidt, Ph.D. Thesis, University of Tübingen, Germany, 1997 – Report FZKA 5917 (1997), Forschungszentrum Karlsrühe.
[30] M. Föller, Ph.D. Thesis, University of Heidelberg, Germany, 1997 – Report FZKA 5918 (1997), Forschungszentrum Karlsruhe.